Available online at www.sciencedirect.com
ScienceDirect
Geochimica et Cosmochimica Acta 73 (2009) 2471–2487
Geochimica et Cosmochimica Acta
www.elsevier.com/locate/gca

XPS spectra of uranyl minerals and synthetic uranyl compounds. I: The U 4f spectrum

M. Schindler [a,*], F.C. Hawthorne [a], M.S. Freund [b], P.C. Burns [c]

[a] Department of Geological Sciences, University of Manitoba, Winnipeg, Man., Canada R3T2N2
[b] Department of Chemistry, University of Manitoba, Winnipeg, Man., Canada R3T2N2
[c] Department of Civil Engineering and Geological Sciences, University of Notre Dame, IN 46556-0767, USA

Received 10 July 2007; accepted in revised form 30 October 2008; available online 14 February 2009

Abstract

The occurrence and binding energies of the U^{6+}, U^{5+} and U^{4+} bands in the U $4f_{7/2}$ peak of 19 uranyl minerals of different composition and structure were measured by XPS. The results suggest that these minerals can be divided into the following four groups: (1) Uranyl-hydroxy-hydrate compounds with no or monovalent interstitial cations; (2) Uranyl-hydroxy-hydrate minerals with divalent interstitial cations; (3) Uranyl-oxysalt minerals with (TO_n) groups (T = Si, P, and C) in which all equatorial O-atoms of the uranyl-polyhedra are shared with (TO_n) groups; (4) Uranyl-oxysalt minerals with (TO_n) groups (T = S and Se), in which some equatorial O-atoms are shared only between uranyl polyhedra. The average binding energies of the $U^{6+}$and U^{4+} bands shift to lower values with (1) incorporation of divalent cations and (2) increase in the Lewis basicity of the anion group bonded to U. The first observation is a consequence of an increase in the bond-valence transfer from the interstitial species (cations, H_2O) groups to the O-atoms of the uranyl-groups, which results in an electron transfer from O to U^{6+}. The second trend correlates with an increase in the covalency of the U—O bonds with increase in Lewis basicity of the anion group, which results in a shift of the electron density from O to U. The presence of U^{4+} on the surface of uranyl minerals can be detected by the shape of the U $4f_{7/2}$ peak, and the occurrence of the U 5f peak and satellite peaks belonging to the U $4f_{5/2}$ peak. The presence of U^{4+} in some of the uranyl minerals and synthetics examined may be related to the conditions during their formation. A charge-balance mechanism is proposed for the incorporation of lower-valence U in the structure of uranyl minerals. Exposure of a Na-substituted metaschoepite crystal in air and to Ultra-High Vacuum results in dehydration of its surface structure associated with a shift of the U^{6+} bands to higher binding energies. The latter observation indicates a shift in electron density from U to O, which must be related to structural changes inside the upper surface layers of Na-substituted metaschoepite.

1. INTRODUCTION

Uranyl-minerals are important in understanding water–rock interactions in U-deposits, and form as products of the oxidation of U mine and mill tailings (Frondel 1958; Finch and Ewing, 1992; Finch and Murakami 1999). They are prominent alteration phases in laboratory experiments involving UO_2 and spent nuclear fuel in a moist, oxidizing environment similar to the proposed repository at Yucca Mountain (Wronkiewicz et al., 1992, 1996; Finn et al., 1996; Finch et al., 1999). Many of the radionuclides released from spent nuclear fuel alteration in a geological repository may be incorporated into uranyl minerals (Burns et al., 1997a, 2004; Burns and Li 2002; Chen et al., 1999, 2000; Douglas et al., 2005). Hence the stability of uranyl minerals and geochemical processes at the mineral–water interface (e.g. dissolution and/or precipitation) may impact the release of radionuclides to the environment.

Surface processes such as dissolution or precipitation can be examined using techniques such as Atomic Force

* Corresponding author. Present address: Department of Earth Sciences, Laurentian University, Sudbury, Ont., Canada P3E 2C6.
E-mail address: mschindler@laurentian.ca (M. Schindler).

0016-7037/$ - see front matter © 2009 Elsevier Ltd. All rights reserved.
doi:10.1016/j.gca.2008.10.042

Microscopy (AFM) and X-ray Photoelectron Spectroscopy (XPS). However, interpretation of XPS spectra from surfaces of uranyl minerals requires a thorough understanding of the spectra. Here, we examine XPS spectra of a series of uranyl minerals of different composition and structure and try to understand what information can be extracted from the resultant spectra.

The U 4f peaks are the strongest and most resolved peaks in the XPS spectrum of U (e.g. Teterin et al., 1981). The U 4f peaks are commonly used to analyze the valence of U on the surface of materials, and, due to their intensity, play an important role in the characterization of adsorbed aqueous uranium species on the surface of minerals (Drot et al., 1998; Froideval et al., 2003; Ilton et al., 2005, 2007; Scott et al., 2005). In the latter context, uranyl minerals are commonly used as reference material for peak shape and full-width at half-maximum (FWHM) of the U^{6+} band in the U 4f peaks (e.g. Ilton et al., 2005 and Froideval et al., 2003). The chemical shift of the U 4f peaks due to the valence of U has been extensively described in the literature, but the effect of surface composition and structure on the chemical shift of these peaks has not been systematically explored over a broad class of uranyl minerals.

The development of new generations of XPS spectrometers with detectors of higher sensitivities, smaller apertures and charge-compensation systems allow measurements of well-resolved high-resolution XPS spectra from single crystals of non-conductors with diameters below 30 μm. In this paper, we will use this capability to examine the effects of the composition and structure of the chemical shift of U^{6+}, U^{5+} and U^{4+} bands in the U $4f_{7/2}$ peaks of uranyl minerals. Furthermore, we will discuss possible incorporation mechanisms for U^{4+} into the structure of uranyl minerals that contain U with a formal valence of 6+. We will use the word *band* to indicate a specific fitted component of the envelope of the U 4f peak or of its satellite peak, and we use the word *species* to indicate U atoms of a specific valence or U-atoms with the same valence but in structurally distinct environments.

1.1. Previous XPS studies of uranyl minerals and natural and synthetic uranates

Amayri et al. (2005a,b) examined the XPS spectra of the uranyl carbonate minerals andersonite, $Na_2Ca(H_2O)_6[(UO_2)(CO_3)_3]$, liebigite, $Ca_2(H_2O)_{10}[(UO_2)(CO_3)_3]$ bayleyite, $Mg_2(H_2O)_{18}[(UO_2)(CO_3)_3]$, and swartzite, $CaMg(H_2O)_{12}[(UO_2)(CO_3)_3]$, and of synthetic $Sr_2[(UO_2)(CO_3)(H_2O)_8$ and $Ba_2[(UO_2)(CO_3)_3](H_2O)_6$. They presented the U 4f spectrum and satellite peaks, and the kinetic energy of the U $6p_{3/2}$ electrons assigned to peaks in the valence band. Teterin et al. (1981) and Froideval et al. (2003) reported XPS data on metaschoepite or a lower-hydrated modification of schoepite. Here, Teterin et al. (1981) gave detailed information for the spectra of the valences and inner U 6p, U 5d, U 5p, U 4f, U 4d, O 2s and O 1s electrons of the mineral. There are numerous XPS investigations for natural and synthetic uranates such as simple UO_X compounds (e.g. Veal et al., 1975; Teterin et al., 1981, Allen and Holmes 1987, Sunder, 1996, Santos et al., 2004), alkali and alkaline-earth uranates (Allen et al., 1978; Bera et al., 1998), and Cs uranates (Van den Berghe et al., 2000). XPS spectra for coffinite $U(SiO_4)_{1-x}(OH)_{4x}$ and synthetic U(IV)-phosphate were reported by Teterin et al. (2000) and Drot et al. (1998), respectively.

2. EXPERIMENTAL METHODS

2.1. Samples

Table 1 lists the uranyl minerals and synthetic compounds with their ideal chemical composition, the average coordination number of U in the structure, the experimental setting (pass-energy/spot size), the peak-shape function and parameters used in the peak fitting process, the observed binding energies and the FWHM of the different bands in the U $4f_{7/2}$ peak. Most minerals were obtained from the William W. Pinch collection at the Canadian Museum of Nature, and from the collection of Gilbert Gauthier. All mineral samples are originally from the Shinkolobwe Mine, Democratic Republic of Congo. Zippeite and magnesium-zippeite were synthesized according to the method of Burns et al. (2003), and becquerelite and Na-substituted metaschoepite were synthesized according to the procedure of Burns and Li (2002) and Klingensmith et al. (2007), respectively. Synthetic α- and β-$[UO_2(OH)_2]$ were grown under hydrothermal conditions at 120 °C for 3 days with a molar ratio of 1:2.5 of uranyl acetate and distilled water. Large single crystals of synthetic liebigite were prepared through evaporation of a 50-mmol L^{-1} $(UO_2)(NO_3)_2$, 100 mmol L^{-1} $CaCl_2$ and 150 mmol L^{-1} Na_2CO_3 solution. All synthetic samples were washed rapidly in distilled water and dried in air. Samples were identified either with a Bruker *P*4 diffractometer fitted with an APEX CCD detector using Mo-Kα radiation or with a Philips PW3830 diffractometer using Cu-Kα radiation and the general chemical composition of a mineral sample was verified with a survey scan (0–1100 eV) in the XPS. Due to the lack of material, the samples of ianthinite, $[U^{4+}{}_2(UO_2)_4O_6(OH)_4(H_2O)_4](H_2O)_5$ and (dehydrated) wyartite were only identified with survey scans in the XPS. Wyartite $Ca[U^{5+}(UO_2)_2(CO_3)O_4(OH](H_2O)_7$ easily dehydrates to dehydrated wyartite, $Ca[U^{5+}(UO_2)_2(CO_3)O_4(OH](H_2O)_3$ in air (Clark, 1960); thus XPS spectra in an Ultra High Vacuum were likely taken from a surface with a composition similar to dehydrated wyartite.

2.2. XPS measurements

The XPS spectra presented in this paper were taken as part of an ongoing investigation of the dissolution of uranyl minerals using Atomic Force Microscopy (AFM), Scanning Electron Microscopy (SEM) and Optical Microscopy (e.g. Schindler et al., 2006a,b, 2007a,b). For XPS measurements of untreated samples, single crystals were cleaved in air and immediately transferred to the XPS. The corresponding XPS spectra were used as references to characterize the XPS spectra of the treated basal surfaces. XPS spectra for single crystals of Na-substituted metaschoepite, metaschoepite, zippeite, magnesium-zippeite and wyartite were taken from non-freshly cleaved surfaces, because the thickness

Table 1
Examined uranyl-compounds, their ideal chemical composition, their origin, experimental setting (analyser pass energy and spot size), type of peak shape function, binding energies, full width at half maximum (FWHM) and proportion (%) of their bands in the U $4f_{7/2}$ peak.

Compound and reference to structure determination	Origin	Pass energy/ spot size/peak shape function	U^{6+1} (±0.1) FWHM (%)	U^{6+2} FWHM (%)	U^{5+} FWHM (%)	U^{4+} FWHM (%)
Uranium minerals containing U^{4+} in their structure						
Uranninite [1] UO_2	Shinkolobwe	160/55 (SY 70)	382.0, 1.65, 14	—	381.2, 1.65, 53	380.3, 1.65, 33
Brannerite [2] $(U,Ca,Ce)(Ti,Fe)O_6$	Shinkolobwe	160/55 (SY 70)	382.1, 1.35, 16	381.4, 1.35, 58	380.6, 1.35, 26	
Ianthinite [3] $[U^{4+}{}_2(UO_2)_4O_6(OH)_4(H_2O)_4](H_2O)_5$	Shinkolobwe	160/55 (SY 70)	381.7, 1.35, 79		380.7, 1.35, 21	
Uranyl-hydroxy-hydrate minerals with divalent interstitial cations						
Becquerelite, [4] $Ca(H_2O)_8[(^{[7]}UO_2)_6O_4(OH)_6]$	Synthetic	160/55 (AS 72, 1.25)	381.1, 1.48, 100	—		—
Becquerelite, [4] $Ca(H_2O)_8[(^{[7]}UO_2)_6O_4(OH)_6]$	Shinkolobwe	160/55 (AS70, 2.7)	381.3, 1.48, 100	—		—
Billietite, [5] $Ba(H_2O)_7[(^{[7]}UO_2)_6O_4(OH)_6]$	Shinkolobwe	40/110 (AS70, 0.95)	381.5, 1.54, 100	—		—
Fourmarierite, [6] $Pb_{1-x}(H_2O)_4[(^{[7]}UO_2)_6O_{3-2x}(OH)_{4+2x}]$	Shinkolobwe	160/55 (AS65, 1.15)	381.4, 1.62, 100	—		—
Curite, [7] $Pb_3(H_2O)_2[(^{[6.75]}UO_2)_4O_4(OH)_3]_2$	Shinkolobwe	160/55 AS(77, 1.20)	381.6, 1.40, 100	—		—
Masuyite, [8] $Pb(H_2O)_3[(^{[7]}UO_2)_3O_3(OH)_2]$	Shinkolobwe	160/55 AS(70, 1.0)	381.1, 1.47, 100	—		—
Uranyl-hydroxy-hydrate compounds with none or monovalent interstitial cations						
α-$[^{[8]}UO_2(1OH)_2]$, [9]	Synthetic	40/110 AS(60, 1)	382.2, 1.28, 95	—		380.7, 1.28, 5
β-$[^{[6]}UO_2(OH)_2]$, [10]	Synthetic	160/55 SY(50)	382.3, 1.30, 96	—		380.5, 1.30, 4
Metaschoepite, [11] $[(UO_2)_4O(OH)_6](H_2O)_5$	Shinkolobwe	160/55 AS(60, 1)	382.0, 1.75, 71	381.4, 1.75, 26		380.4, 1.75, 3
Na-substituted metaschoepite, [12] $Na_{1-x}[(^{[7]}UO_2)_4O_{2-x}(OH)_{5+x}]\,(H_2O)_n$	Synthetic	160/55 SY(70)	382.1, 1.3, 68	381.3, 1.3, 25		380.5, 1.3, 7
untreated						
+HCl, pH 2, 2 min	Synthetic	160/55 SY(70)	382.1, 1.3, 62	381.3, 1.3, 22		380.3, 1.3, 16
+6 months on air	Synthetic	160/55 SY(70)	382.2, 1.3, 49	381.9, 1.3, 42		380.3, 1.3, 9
+1 week UHV + 10 h X-rays	Synthetic	160/55 SY(70)	382.6, 1.3, 46	382.1, 1.3, 42		380.7, 1.3, 12
Uranyl-oxy-salt minerals in which all equatorial O-atoms are shared with (TO_n) groups						
Liebigite, [13] $Ca_2[(UO_2)(CO_3)_3](H_2O)_{11}$	Synthetic	40/110 SY(80)	381.9, 1.26, 95	—		380.2, 1.26, 5
Uranophane, [14] $Ca(H_2O)_5[(^{[7]}UO_2)(SiO_3(OH)]_2$	Shinkolobwe	80/55 SY(50)	382.1, 1.20, 81	—		380.4, 1.20, 19
Uranophane-β, [15] $Ca(H_2O)_5[(^{[7]}UO_2)(SiO_3(OH)]_2$	Shinkolobwe	SY(70) 160/55	382.0, 1.2, 95	—		380.4, 1.2, 5
Soddyite, [16] $[(UO_2)_2(SiO_4)(H_2O)_2]$	Shinkolobwe	SY(70) 160/55	382.0, 1.4, 90			380.2, 1.4, 10
Metatorbernite, [17] $Cu(H_2O)_8[(^{[6]}UO_2)(PO_4)]_2$	?	40/110 AS(60, 1)	381.9, 1.31, 100	—		—
Uranyl-oxy-salt minerals in which some equatorial O-atoms are exclusively shared between (UO_2O_7) polyhedra						
Zippeite, [18] $K_3(H_2O)_3[(^{[7]}UO_2)_4(SO_4)_2O_3(OH)]$	Synthetic	160/55 AS(85, 1.2)	381.7, 1.71, 100	—		—
Magnesium-zippeite, [18] $Mg(H_2O)_{3.5}[(^{[7]}UO_2)_2(SO_4)O_2]$	Synthetic	160/55 AS(85, 1.2)	381.6, 1.57, 92	—	380.5, 1.57, 8	
Marthozite, [19] $Cu(H_2O)_8[(^{[7]}UO_2)_3(SeO_3)_2O_2]$	?	80/110 AS(53, 0.83)	381.5, 1.63, 100	—		—
Dehydrated Wyartite, [20] $Ca[U^{5+}(UO_2)_2(CO_3)O_4(OH)](H_2O)$	Shinkolobwe	160/55 SY 70	381.7, 1.45, 100			
Dehydrated Wyartite, [20] $Ca[U^{5+}(UO_2)_2(CO_3)O_4(OH)]\,(H_2O)_3$	Shinkolobwe	160/55 SY 70	381.7, 1.45, 88			380.2, 1.45, 12

[1] Goldschmidt and Thomassen (1923); [2] Szymanski and Scott (1982), [3] Burns et al. (1997b), [4] Burns and Li (2002), [5] Finch et al. (2006), [6] Piret (1985), [7] Li and Burns (2000) [8] Burns and Hanchar (1999), [9] Taylor (1971), [10], Taylor and Bannister (1972), [11] Weller et al. (2000), [12] Klingensmith et al. (2007) [13] Mereiter 1982, [14] Ginderow (1988), [15] Viswanathan and Harneit (1986), [16] Demartin et al. (1992), [17] Locock and Burns (2003), [18] Burns et al. (2003), [19] Cooper and Hawthorne (2001), [20] Hawthorne et al. (2006).

of their crystals did not allow cleaving parallel to the basal face. However, these crystals were washed in distilled water and dried in a N_2 air stream before transfer into the XPS chamber.

It is important to emphasize here that all XPS data were measured exclusively on the surface of single crystals, because previous published data on the XPS spectra of uranyl compounds (see above) were taken from finely dispersed powdered samples. Advantages of single crystals are the amount of material required (an important issue if one works with rare mineral samples such as metaschoepite or billietite) and the known identity, orientation and quality of the samples. Furthermore, the XPS can be combined with AFM examination, and data on the relief and chemical composition of a surface can be obtained.

Spectra of the U 4f, 6p and 5f electrons were taken with a Kratos Axis Ultra X-ray Photoelectron Spectrometer (XPS) with a magnetic-confinement charge-compensation system. Advantages of this system with regard to insulators (e.g. uranyl minerals) have been described in detail by Nesbitt et al. (2004). Spectra were collected in high-resolution scans using monochromatic Al-Kα radiation (1486.6 eV) and the charge-compensation system. Spectra for the U 4f (370–410 eV) and 6p and 5f (−5 to 25 eV) electrons were recorded using 20 sweeps and scan rates per sweep of 80 s and 300 ms, respectively. The spectra of crystals with an average lateral dimension below 100 μm (on the basal surface) were recorded with a constant analyser pass-energy of 160 eV and a spot size of 55 μm, and spectra of crystals with an average lateral dimension above 100 μm were collected with a pass energy of 40 eV and a spot size of 110 μm.

To avoid contributions from photoelectrons emitted from the sample holder, each crystal was centered in the spot of the aperture by imaging emitted U 4f electrons from its surface. The electrostatic sample charging (that remained after charge compensation) was corrected by adjusting the binding energy of the 1s photoelectrons of adventitious carbon on the sample surface to 285 eV (Wagner et al., 1979).

3. THE U 4f SPECTRA

The U $4f_{7/2}$ and $4f_{5/2}$ peaks occur around 380 and 390 eV, respectively. The spin–orbit interaction separates these two levels by around 10.9 eV for uranium minerals (Fig. 1). The U $4f_{7/2}$ peak position may vary as dictated by the crystal structure, the influence of which is due to the nearest-neighbour ions.

Shake-up satellites are small peaks that are produced by photoelectrons that have lost part of their initial energy to a valence-band electron. When a core-level electron is expelled, an electrostatic potential is experienced by the valence electrons. They are excited to a higher empty orbital or are knocked off to the continuum almost at the same time. The energy difference between the ground state and the higher orbital defines the difference in position between the satellite peak and the photoelectron peak. The position of the satellite peak also depends on the valence of the element and the type and number of its nearest-neighbour ions. A recent and more detailed discussion on the satellites peaks of the U 4f spectrum can be found in Ilton et al. (2007).

For uranium, both U 4f core-level peaks show satellites at higher binding energies: 6–7 eV for U^{4+}, 7.8–8.5 eV for U^{5+} and 4 and 10 eV for U^{6+} (e.g. Keller and Jorgensen, 1975; Teterin et al., 1981; Bera et al., 1998; Van den Berghe et al., 2000; Santos et al., 2004; Ilton et al., 2007). Some of the satellites of the U $4f_{7/2}$ peak are buried in the intense U $4f_{5/2}$ peak or may appear as a shoulder, which may lead to incorrect interpretation regarding the occurrence and fractions of the different bands. Hence, satellites of the U $4f_{7/2}$ peak and the U $4f_{5/2}$ peak are normally not considered for spectral interpretation, and one instead uses the satellites of the U $4f_{5/2}$ peaks and the shape of the U $4f_{7/2}$ peak for the determination of the U^{6+}, U^{5+} and U^{4+} bands.

Previously reported binding energies for U^{6+}, U^{5+} and U^{4+} in the U $4f_{7/2}$ peak of mixed-valent U-compounds vary with the chemical composition of the compounds examined. However, separations between the bands are similar for many compounds and have average values of 0.9 eV for U^{6+}–U^{5+} and 0.6 eV for U^{5+}–U^{4+} (e.g. Bera et al., 1998; Santos et al., 2004).

3.1. Peak function and asymmetry of the U $4f_{7/2}$ spectrum

Fitting functions commonly use a mixture of a Gaussian and Lorentzian functions. The software Vision 2.26 (2006) uses a Gaussian and Lorentzian function developed by Sherwood (1990):

$$F(x) = \text{peakheight} \Big/ \left[1 + M(x - x_o)^2/\beta^2\right] \exp\left\{(1 - M)\left[(\ln 2)(x - x_o)^2\right] \Big/ \beta^2\right\} \quad (1)$$

Here, x_o is the peak centre, β is the parameter that controls the FWHM-value and M is the Gaussian/Lorentzian mixing ratio.

The region after a XPS peak is dominated by extrinsic effects such as losses experienced by the photoelectron during the transport to the exposed surface (Castle, 2002). These losses result in a sharp rise in the background at the peak, which can be corrected using proposed background corrections by Shirley (1972) or Tougaard (1996). The region close to and including the peak is dominated by intrinsic effects, such as losses associated with the concomitant excitation of an outer electron during photoionization of the core. These losses can result in asymmetric peak shapes and sloping backgrounds at the higher binding energy side, which can be often found in XPS spectra of transition elements (Doniach and Sunjic, 1970; Castle and Salvi, 2001). Software packages such as Vision 2.26 (2006) contain an asymmetric tail function that attempts to approximate asymmetric photoelectron peaks at the higher binding energy side. This asymmetric tail function (AS 1, 2) contains two parameters: the first parameter defines the Gaussian–Lorentzian peak shape and the second parameter is the exponential parameter ET used in the exponential part of the tail function T developed by Sherwood (1990)

$$T = \exp(-\text{Dx ET}) \quad (2)$$

where, Dx is the separation from the peak centre.

The peak function at the lower binding-energy side is chosen to have no tail and can be represented by Eq. (1)

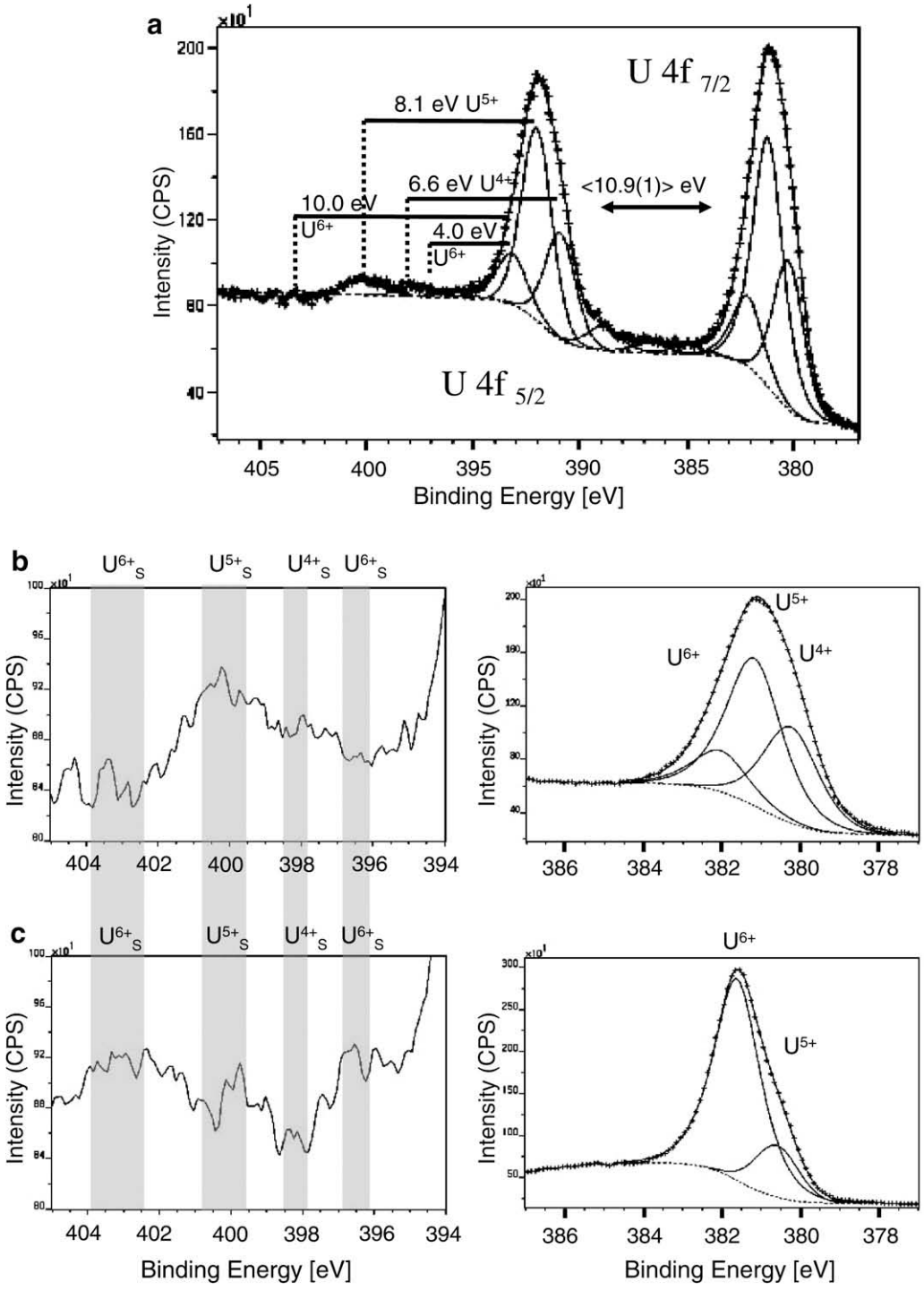

Fig. 1. (a) The U $4f_{5/2}$ and U $4f_{7/2}$ regions of the XPS spectra for a uraninite crystal from Shinkolobwe, Republic of Congo. (b and c) Satellite peaks in the region after the U $4f_{5/2}$ peak (left) and proportion of the bands in the U $4f_{7/2}$ spectra (right) from the spectrum above (b) and from an ianthinite crystal (c). The vertical and horizontal lines show the anticipated satellite peaks for U^{4+}, U^{5+} and U^{6+}.

whereas the peak function at the higher binding-energy side contains the additional parameter T. The overall FWHM-value of a fitted peak depends among other experimental factors on the Gaussian–Lorentzian peak-shape ratio and the exponential factor ET in the tail function T (Sherwood, 1990); i.e. the higher the Lorentzian character and the smaller ET, the higher the resulting FWHM-value.

3.2. Analyzer resolution and variation in binding energies

The analyzer resolutions for different pass energies and spot sizes were determined using the Ag $3d_{5/2}$ line spectrum. Furthermore, C 1s and U $4f_{7/2}$ spectra of metatorbernite, $Cu(H_2O)_8[(^{[6]}UO_2)(PO_4)]_2$ were taken at different pass energies and spot sizes in order to compare their resolution with

those of the Ag $3d_{5/2}$ line spectra. Table 2 lists FWHM-values of the Ad $3d_{5/2}$ spectra and binding energies and FWHM values of the C 1s and U $4f_{7/2}$ spectra for three different experimental settings.

The U $4f_{7/2}$ spectra have an asymmetric tail at the higher binding-energy side, demanding the fitting of the spectra with an asymmetric peak-tail function. However, the U $4f_{7/2}$ spectra were also fitted without asymmetric peak-shape function in order to compare FWHM-values from fittings with different peak-shape functions.

Inspection of the FWHM-values for the Ag $3d_{5/2}$, C 1s and U $4f_{7/2}$ spectra shows that (a) differences in resolution between the settings 40/110 and 160/55 are smaller in the case of metatorbernite than for metallic Ag and (b) peak fittings with an asymmetric peak tail function result in larger FWHM-values than with a simple Gaussian–Lorentzian peak shape function (Table 2). The latter observation is only true for small exponential factors (ET) in the tail functions, whereas larger factors of ET do not significantly increase the FWHM-value in comparison to a Gaussian–Lorentzian peak shape function.

The estimated standard deviation for the binding energy of an U $4f_{7/2}$ peak is ±0.1 eV, which is the sum of standard deviations from the peak fittings of the U $4f_{7/2}$ and C 1s spectra at different experimental settings (Table 2). The latter spectrum is used for calibration of the U $4f_{7/2}$ spectrum (see above) and its standard deviation (±0.02 eV) is determined on the basis of multiple fittings of its envelope.

3.3. Peak fitting

Shirley background corrections (Shirley, 1972) and a Gaussian–Lorentzian peak shape (70 ± 20% Lorentzian) were used to fit all U $4f_{7/2}$ spectra. In the case of an asymmetric spectrum, an additional asymmetric tail function (AS 1, 2) was included in the fitting process (Vision 2.2.6, 2006). The exponential factor, ET in the tail function varied from 0.85 (for prominent asymmetric tails) to 3.1 (for nearly symmetrical peaks).

We considered in the peak fitting process the change in FWHM-value of U^{6+} with pass energy, spot size and the applied peak-shape function (Gaussian–Lorentzian peak ratio and the exponential factor ET) and therefore did not constrain FWHM-values to specific ranges. However, we used the FWHM-values of torbernite for the different experimental settings and peak shape functions as a guide for the peak fitting of other U 4f spectra. Different bands under the same U $4f_{7/2}$ envelope were fitted with identical FWHM-values and peak-shape functions.

3.4. Satellite peaks and the spectra of U $6p_{3/2}$, valence band and U 5f

The U 4f spectrum of uraninite (UO_2) is suited to describe the occurrence and location of satellite peaks because the oxidized surface of the mineral normally contains U in the valences 4+, 5+ and 6+ (Sunder et al., 1996). Fig. 1a shows the U 4f spectrum of a uraninite crystal in which we indicated typical distances between satellite peaks and the bands of U^{6+} (4 and 10 eV), U^{5+} (~8 eV) and U^{4+} (6.6 eV). The spectrum indicates a strong satellite peak 8.1 eV apart from the major band in the U $4f_{5/2}$ peak, indicating that U^{5+} is the dominant species on the surface. Fig. 1b shows a higher magnification of the spectrum in the range 394–405 eV. Closer inspection of this spectrum shows the occurrence of small satellite peaks corresponding to U^{4+} (6.6 eV) and U^{6+} (10 eV) whereas no satellite peak is resolved around 4 eV. The U $4f_{7/2}$ peak was then fitted into U^{6+}, U^{5+} and U^{4+} bands (FWHM = 1.65 eV) with separations of 0.8 eV (U^{6+}–U^{5+}) and 0.9 eV (U^{5+}–U^{4+}), in accordance with literature values for mixed-valent U^{6+}–U^{5+}–U^{4+} uranates (see above).

Fig. 1c shows the U $4f_{7/2}$ spectrum and the satellite peaks of ianthinite, $[U^{4+}{}_2(UO_2)_4O_6(OH)_4(H_2O)_4](H_2O)_5$ (Burns et al., 1997b). The U $4f_{7/2}$ spectrum contains a prominent U^{6+} band which is separated by 1.0 eV from a band at the lower binding energy side. This separation agrees with reported values for separations of U^{6+} and U^{5+} bands (see above). Inspection of the satellite peaks shows the occurrence of peaks at 4 and 10 eV from the U^{6+} band and a small satellite peak 8.4 eV apart from the U^{5+} band, in accordance with the observed bands in the U $4f_{7/2}$ peak.

Assignment of U^{4+} and U^{5+} valences is more difficult for spectra taken from small crystals. Small crystals of uranyl minerals commonly produced XPS spectra with a low signal to noise ratio, which makes it difficult to resolve the satellite peaks for U^{6+}, U^{5+} and U^{4+}. Furthermore, the proportion of the U^{4+} and U^{5+} bands are in general very low in the envelope of the U $4f_{7/2}$ spectra of uranyl minerals. Hence, their corresponding satellite peaks were almost always not resolved and could not be used as an unequivocal proof for the occurrence of U^{5+} and U^{4+}. In those cases, we used the separation of the bands in the U $4f_{7/2}$ envelope and the ratio of intensities be-

Table 2
FWHM values for Ag $3d_{5/2}$ of metallic silver and binding energies with estimated standard deviations and FWHM-values for the C 1s and U $4f_{7/2}$ spectra of metatorbernite at different experimental settings and for peak fittings using a Gaussian–Lorentzian peak shape (G/L) or an asymmetric peak shape function AS(60, 1).

Pass energy/ spot size	Ag $3d_{5/2}$ G/L peakFWHM	C 1s (eV) G/L peak	FWHM (eV)	U $4f_{7/2}$ AS(60, 1) (eV)	FWHM (eV) AS(60, 1)	FWHM symmetric G/L peak (eV)
40/110	0.68	282.54	1.15	381.88	1.31	1.14
160/55	1.11	281.58	1.34	382.02	1.62	1.43
160/110	1.63	281.86 Std: ±0.02[a]	1.55	381.96 <381.96> Std: ±0.08	2.04	1.83

[a] Based on multiple fittings at different experimental settings.

tween the U 5f peak and the O2p peak in the valence bands as indicators.

Fig. 2a–c show U $4f_{7/2}$ spectra and spectra taken close to the Fermi level from crystals of uraninite, brannerite, (U,Ca,Ce)(Ti,Fe)O_6 and Na-substituted metaschoepite, $Na_{1-x}[([^{[7]}UO_2)_4O_{2-x}(OH)_{5+x}]$. The area close to the Fermi level can be divided into three distinct parts:

(1) the U $6p_{3/2}$ peak in the range of 16–20 eV,
(2) the U 5f peak at ~1.5 eV and
(3) the O 2p peak at 3–8 eV.

In compounds where uranium is hexavalent, the U 5f level is empty and the XPS spectra accordingly show no peak (Veal et al., 1975; Teterin et al., 1981). The intensity of the U 5f line in the XPS spectra of the uranium oxides is proportional to the number of 5f electrons with anti-bonding characters (U^{4+} and U^{5+} have electronic configurations of $5f_2$ and $5f_1$, respectively). Teterin et al. (1981) showed for UO_x compounds that, the intensity of the U 5f line decreases as O increases. The valence band is due to dominantly O 2p orbitals that have bonding character with the U 5f orbitals. Ilton et al. (2007) showed that an increase in the proportions of U^{5+} and U^{4+} result in an increase in the ratio between the intensities of the U 5f peak and the O 2p peak as a consequence of the decrease in the number of uranyl bonds and an increase in the number of 5f electrons with anti-bonding character.

The U $6p_{3/2}$ peak splits with the reduction in symmetry (Veal et al., 1975) of the uranium polyhedra from a cubic coordination in UO_2 (Goldschmidt and Thomassen, 1923) to a distorted octahedral coordination with longer equatorial U—O and shorter uranyl-bonds in e.g. γ-UO_3 (Loopstra et al., 1977). This reduction in symmetry leads to the asymmetry of the electrical field surrounding the central uranium ion and the resulting splitting of the U $6p_{3/2}$ peak can be used to determine the equatorial U—O bond length (Veal et al., 1975; Nefedov et al., 1996). Note that, a reduction in symmetry can be also the result of a phase transition and that the splitting of the U $6p_{3/2}$ peak does not necessarily indicate the presence of U^{6+} and U^{5+} in the structure of a U^{4+} mineral.

Fig. 2a shows the proportions of the U^{6+}, U^{5+} and U^{4+} bands in the U $4f_{7/2}$ peak, the splitting of the U $6p_{3/2}$ peak, and the ratio between the intensities of the U 5f peak and the O 2p peak for an oxidized surface of uraninite. We

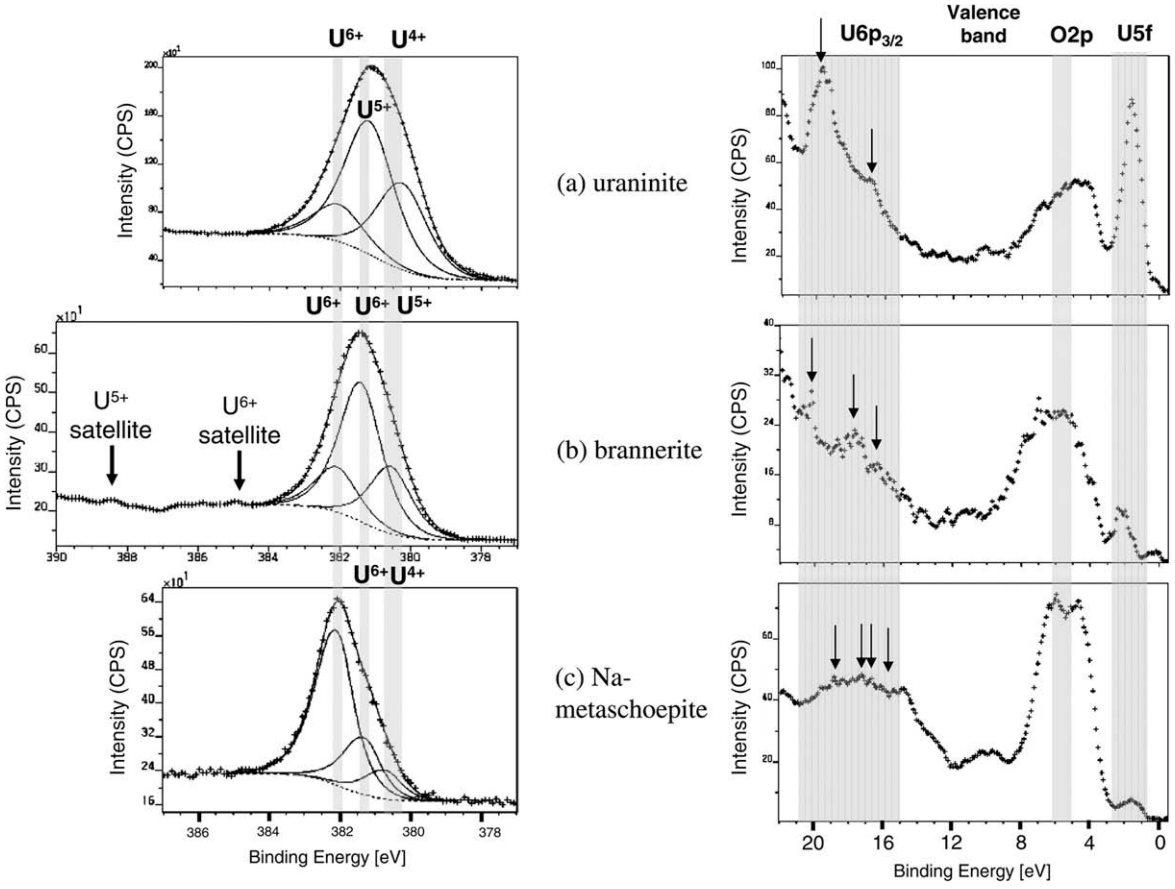

Fig. 2. XPS spectra showing the proportion of bands in the U $4f_{7/2}$ peaks and the electronic levels within 22 eV of the Fermi level for (a) uraninite with U^{4+}, U^{5+} and U^{6+}, (b) brannerite and (c) Na-substituted metaschoepite with two different U^{6+} bands. The different levels and bands are labelled and their locations are indicated with grey-shaded vertical bars. The thickness of the grey-shaded vertical bars indicates the variation in binding energy between identical bands in both spectra. The crystal-field splitting of the U $6p_{3/2}$ level is indicated with arrows (see text for details).

can now compare these observed features in the spectra of uraninite with the corresponding spectra of brannerite and metaschoepite for which satellite peaks of U^{4+} (brannerite) and U^{4+}+ U^{5+} (metaschoepite) are not resolved in the U 4f spectrum. The U $4f_{7/2}$ spectrum of brannerite resembles the spectrum of uraninite and contains a prominent band at 381.4 eV and smaller bands at 382.1 and 380.6 eV. Hence, one would expect similar spectra of U $6p_{3/2}$, O 2p and U 5f for brannerite. However this is not the case (Fig. 1b): The splitting of the U $6p_{3/2}$ peak is more enhanced and the ratio between the intensities of U 5f and the O 2p is much smaller in comparison to the spectrum of uraninite. Hence, the prominent band in the U $4f_{7/2}$ peak must be assigned to a U^{6+} component, indicating the occurrence of two U^{6+} species in different structural environments. The band at 380.6 eV is 0.8 eV from the prominent U^{6+} bands at 381.4 and 7.8 eV from a satellite peak at 388.4 eV (Fig. 2b). Both distances agree with reported U^{6+}–U^{5+} and U^{5+}–satellite peak distances and thus, the band at 380.6 eV must be assigned to U^{5+}. In the case of Na-substituted metaschoepite, the U $6p_{3/2}$ peak shows a large splitting and the ratio between the U 5f and the O 2p peak is extremely low (Fig. 2c), indicating that the bands at 382.1 and 381.3 eV (Table 1) must be assigned to U^{6+} species. The band at 380.6 eV is 0.7 eV and 1.5 eV apart from the U^{6+} bands at 381.3 and 382.1 eV, respectively. These distances agree with reported U^{6+}–U^{5+} and U^{6+}–U^{4+} distances in U $4f_{7/2}$ spectra and thus, a specific valence cannot be assigned to the band at 380.6 eV.

We can summarize that U $6p_{3/2}$ and U 5f spectra help to determine the ratio between U^{6+} and (U^{5+} + U^{4+}) bands in the U $4f_{7/2}$ envelope, but they do not show whether small proportions of either U^{5+} or U^{4+} are present on the surface of a uranyl-mineral.

3.5. Effect of Ultra-High Vacuum and an X-ray beam on the surface of uranyl minerals

Allen and Holmes (1987), Wersin et al. (1994) and Schueneman et al. (2003) showed that an Ultra-High Vacuum (UHV) can slowly reduce U^{6+} to U^{5+} and U^{4+}. Allen and Holmes (1987) showed that in the case of α-UO_3, reduction of U^{6+} is most likely the product of the combination of UHV and bombardment with X-rays, and that the degree of reduction increases with the time the sample is in the spectrometer (0.5–8.0 h). Ilton et al. (2007) studied in detail the beam-induced reduction of U^{6+} in adsorbed U-species and/or a precipitated uranyl-hydroxy-hydrate on the surface of annite, an iron-rich trioctahedral mica. They monitored the U 4f, U 5f and the satellite peaks of the U 4f peaks during a 26 h experiment and observed a continuous reduction of U^{6+} to U^{5+} and U^{4+}.

The uranyl minerals examined here were in the spectrometer between 12 and 72 h. Hence, it was necessary to test if reduction of U^{6+} on the surface of the uranyl minerals occurs over this timeframe. We tested billietite $Ba(H_2O)_7[(^{[7]}UO_2)_6O_4(OH)_6]$, a uranyl mineral without any U^{4+} and U^{5+} components in the U $4f_{7/2}$ envelope. We stored a crystal of billietite in the XPS instrument at 10^{-10} torr for 1 week and subsequently exposed the sample to X-rays for 10 h. Comparison of the U $4f_{7/2}$ spectra taken before and after the treatment showed no change in the envelope of billietite. This observation differs from the beam/UHV induced reduction observed in the cited studies above.

4. RESULTS

The chemical shifts of the $U^{6+}$and U^{4+} bands in the U $4f_{7/2}$ peak of the uranyl minerals are between 381.0–382.3 and 380.2–380.7 eV, respectively. Closer inspection of Table 1 indicates that the bands of the U $4f_{7/2}$ peaks occur at similar positions for uranyl minerals of similar composition and/or structure.

Uranyl minerals are commonly classified according to the degree of polymerization of their structural units (framework, sheet, chain, cluster, isolated polyhedron) and on the topology of their sheets of polymerized uranyl-polyhedra (Burns et al., 1996, Burns 1999, 2005). The uranyl-minerals examined here may be divided into the following four groups on the basis of their structure and chemical composition:

(1) Uranyl-hydroxy-hydrate compounds with no interstitial cations or monovalent interstitial cations;
(2) Uranyl-hydroxy-hydrate minerals with divalent interstitial cations;
(3) Uranyl-oxysalt minerals with (TO_n) groups (T = Si, P and C) in which all equatorial O-atoms of the uranyl polyhedra are shared with (TO_n) groups;
(4) Uranyl-oxysalt minerals with (TO_n) groups (T = S and Se) in which some equatorial O-atoms are shared only between uranyl polyhedra.

Chemical shifts and the occurrence of U^{5+} and U^{4+} bands will be now discussed for each group and then compared with observations of natural and synthetic uranates.

4.1. Uranyl-hydroxy-hydrate compounds with no or monovalent interstitial cations

In the U $4f_{7/2}$ peaks of this group, the U^{6+} bands occur at 382.00–382.3 eV with an average value of <382.1> eV, (Table 1 and Fig. 3). Here, the observed binding energies of 382.05 and 382.0 eV for U^{6+} in Na-substituted metaschoepite and metaschoepite agree well with the reported binding energy of 382.0 eV for U^{6+} in synthetic metaschoepite (Froideval et al., 2003).

In the spectra of α-$[^{[8]}UO_2(OH)_2]$ and β-$[^{[6]}UO_2(OH)_2]$, a second band occurs between 380.5 and 380.7 eV. This band is separated from the U^{6+} band by 1.5 and 1.8 eV; in accord with values reported for distances between U^{6+} and U^{4+} bands (see above).

Additional bands occur at 381.4 and 381.3 eV in the U 4f spectra of metaschoepite and Na-substituted metaschoepite, respectively. As shown above for Na-substituted metaschoepite, the ratio between the intensities of U 5f peak and the valence band clearly indicate for both minerals that these bands represent a second U^{6+} species (see below). The occurrence of two U^{6+} bands and the absence of satellite peaks for U^{5+} and U^{4+} in the U 4f spectra made it impossible to assign a valence

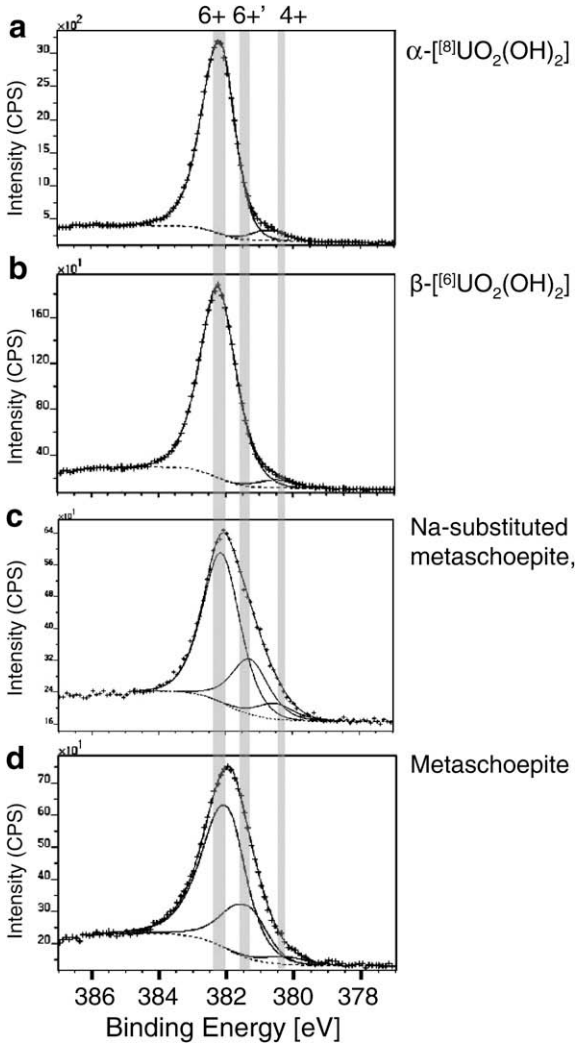

Fig. 3. The U $4f_{7/2}$ spectra for uranyl-hydroxy-hydrate minerals with or without monovalent interstitial cations. The location of the U^{6+} and U^{4+} bands and their variations in binding energies indicated with vertical grey-shaded bars.

to the band at 380.5–380.7 eV. However, spectra taken from a Na-substituted metaschoepite crystal, which has been treated with an HCl solution of pH 2 and exposed to air for 6 months, suggest that the latter band belongs to a U^{4+} species (see below for details).

The polymorphs α- and β-[$(UO_2)(OH)_2$] contain U in [8]- and [6]-coordination, respectively (Fig. 3 and Table 1). Similar binding energies of the U^{6+} band in the spectra of each compound indicate that the coordination number of U does not affect the chemical shift of the U $4f_{7/2}$ peak.

4.2. Uranyl-hydroxy-hydrate minerals with divalent interstitial cations

The U^{6+} band in the U $4f_{7/2}$ peaks of these minerals occurs between 381.0 and 381.6 eV with an average value of <381.3> eV (Table 1 and Fig. 4). There was no indication of U^{5+} or U^{4+} in the U 4f and 5f spectra. In addition, almost all U $4f_{7/2}$ peaks have an unsymmetrical shape to the higher-energy side and their spectra were fitted with the asymmetric peak shape function (Table 1).

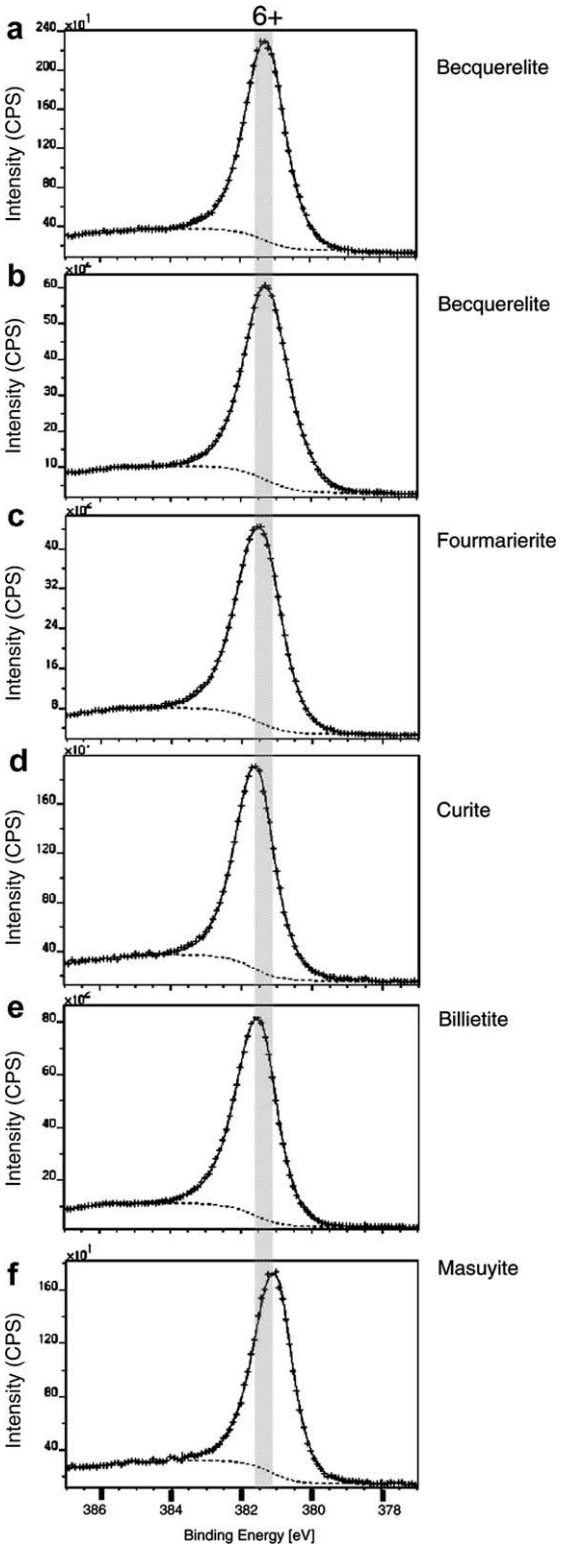

Fig. 4. The U $4f_{7/2}$ spectra for uranyl-hydroxy-hydrate minerals with divalent interstitial cations; location of the bands and their variations in binding energies are indicated with vertical grey-shaded bars.

4.3. Uranyl oxysalt minerals in which all equatorial O-atoms are shared with (TO_n)

The binding energies for U^{6+} and U^{4+} in minerals of this group range from 381.9 to 382.2 eV and from 380.2 to 380.4 eV with average values of <382.0> and <380.4> eV, respectively (Table 1 and Fig. 5). The average separation between both bands is <1.6> eV, which agrees with the values reported for mixed-valent U-compounds (see above). The binding energies for U^{6+} and U^{4+} are similar to those observed for the uranyl-hydroxy-hydrates with or without monovalent interstitial cations.

The spectrum for soddyite was assigned to this group, although one equatorial ligand in the uranyl-polyhedra is a (H_2O) group. However, the uranyl-polyhedra share four out of the five equatorial ligands with silica tetrahedra and the equatorial H_2O group is not shared with another uranyl-polyhedra. Furthermore, (H_2O) has a similar Lewis base strength as $(CO_3)^{2-}$ and $(SiO_4)^{4-}$ (see below).

The observed binding energy of 381.9 eV in synthetic liebigite agrees with the previous reported value of 381.8 eV (Amayri et al., 2005a).

4.4. Uranyl-oxy salt minerals in which some equatorial O-atoms are shared only between uranyl polyhedra

The binding energies for U^{6+} in the U $4f_{7/2}$ peak of these minerals are between 381.5 and 381.7 eV with an average value of <381.6> eV (Fig. 6 and Table 1). The U 4f envelope of Mg-zippeite clearly shows a shoulder on the lower binding energy side and an additional band had to be included in the fitting process. This band is 1.1 eV apart from the U^{6+} band, suggesting the presence of a small fraction of U^{5+}. A satellite peak associated with such a small proportion of U^{5+} would be not resolved in the U $4f_{5/2}$ spectrum, in accord with our observations.

Interesting are the spectra of (dehydrated) wyartite which contain U^{5+} in its structure and which oxidizes quickly in air (Gauthier et al., 1989). Fig. 6d shows the U $4f_{7/2}$ spectrum of a non-freshly cleaved sample of (dehydrated) wyartite, which indicates that the surface contains exclusively U^{6+}. A spectrum of a freshly-cleaved sample of (dehydrated) wyartite contains an additional band at 380.2 eV (Fig. 6e). This band is 1.5 eV apart from the U^{6+}, which indicates the presence of U^{4+} rather than U^{5+}. This observation however does not necessarily imply that, the structure of (dehydrated) wyartite contains U^{4+} rather than U^{5+}. It simply indicates that all of the U^{5+} has been oxidized on the surface of the mineral and that the presence of U^{4+} may indicate a disproportionation of U^{5+}. The time between cleaving the crystal and its transfer to the vacuum chamber of the XPS was approximately one minute, suggesting very rapid oxidation (or disproportionation) of U^{5+} on the freshly cleaved surface. This rapid oxidation of U^{5+} on the surface of wyartite seems inconsistent with the presence of U^{5+} on the surface of uraninite, ianthinite and brannerite (see above). However, the kinetics of oxidation will depend on the structural environment of the corresponding cation and anion. For uraninite, ianthinite and brannerite, the structural environments of U^{5+} are very different from that in wyartite. In the wyartite structure, U^{5+} shares an edge with a (CO_3) triangle, whereas on the surfaces of uraninite, ianthinite and brannerite, U^{5+} does not bond to any complex anion.

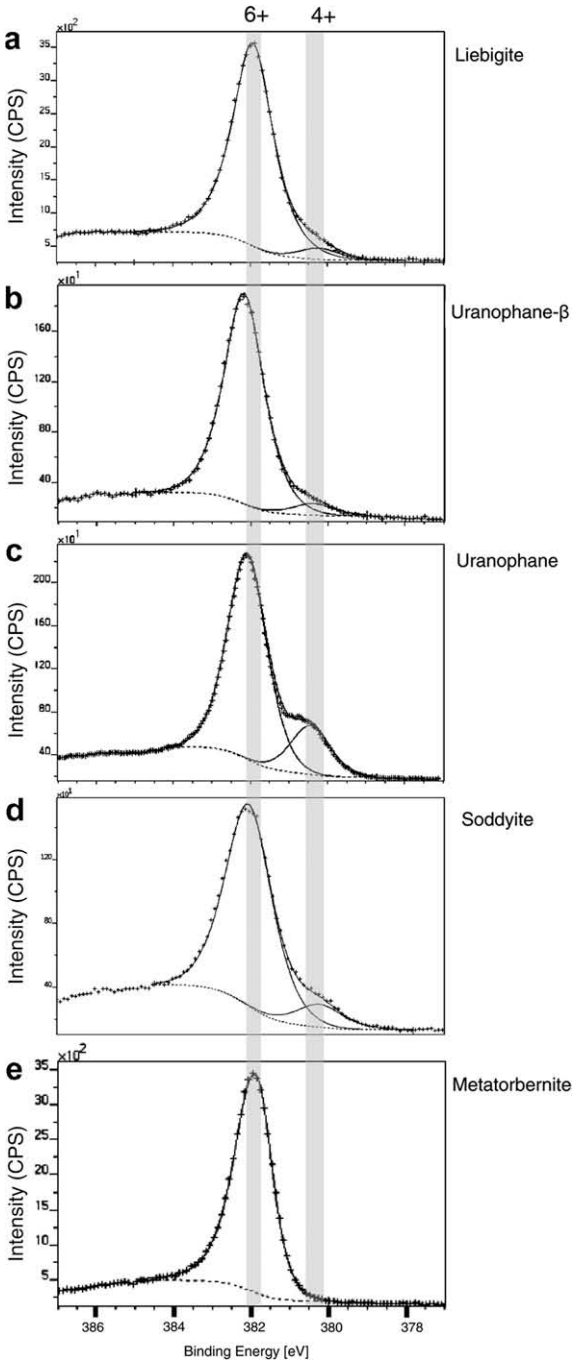

Fig. 5. The U $4f_{7/2}$ spectra for uranyl-oxy-salt minerals with (TO_n) groups (T = Si, P, and C) in which all equatorial O-atoms of the uranyl-polyhedra are shared with (TO_n) groups (Note that the structure of soddyite contains a non-shared H_2O group as an equatorial ligand in the uranyl-polyhedra); location of the bands and their variations in binding energies are indicated with vertical grey-shaded bars.

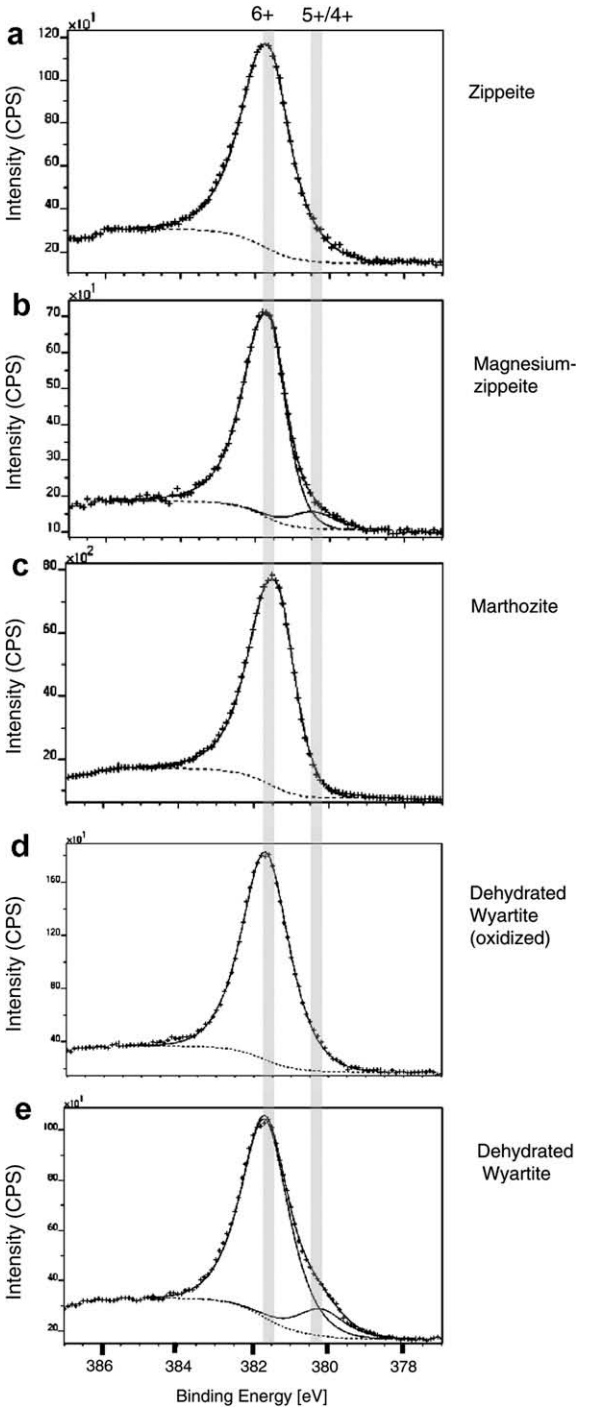

Fig. 6. The U $4f_{7/2}$ spectra for uranyl-oxy-salt minerals with (TO_n) groups (T = S and Se) in which some equatorial O-atoms are exclusively shared between uranyl-polyhedra; location of the bands and their variations in binding energy are indicated with vertical grey-shaded bars.

5. DISCUSSION

We are now in the position to compare the observed binding energies of the bands in the U $4f_{7/2}$ peaks of the uranyl minerals with those in uranates. The binding energies for U^{6+} in α-, β-, γ- and δ-UO_3 are in the range 382.0–382.1 eV (Allen and Holmes 1993) and the binding energy for U^{4+} in UO_2 is in the range 379.9–380.4 eV (on the basis of the C 1s peak at 285 eV; Bera et al., 1998; Van den Berghe et al., 2000; Schueneman et al., 2003). The average separation between both peaks is <1.7> eV, in accord with the observation of Allen and Holmes (1993). For alkali and alkaline-earth MUO_x compounds (M = Na, Li, Rb, Tl^+, Sr, and Ba), Bera et al. (1998) reported binding energies for U^{6+}, U^{5+} and U^{4+} in the range 381.4–381.9, 380.8–380.9 and 380.0–380.4 eV, respectively. The average separations between the peaks are 0.9 eV for U^{6+}–U^{5+} and 0.6 eV for U^{5+}–U^{4+}.

Comparison of the binding energies between uranyl minerals and uranates indicates that the presence of alkali and alkaline-earth cations shifts the U^{6+} band to lower binding energy; i.e. from <382.0> eV for the polymorphs of UO_3 to <381.7> eV for MUO_x compounds, and from <382.1> eV for uranyl-hydroxy-hydrates with zero or small amounts of monovalent interstitial cations to <381.3> eV for the uranyl-hydroxy-hydrate minerals with divalent interstitial cations. The explanation of this shift is not trivial and we will therefore focus first on the observed shift of the U 4f peak for minerals with divalent cations.

5.1. Binding-energies of the U 4f spectra for minerals with divalent cations

Uranyl minerals with divalent interstitial cations are (1) uranyl-hydroxy-hydrates, (2) uranyl oxysalts containing only (TO_n) oxyanions, and (3) uranyl oxysalts containing both (TO_n) oxyanions and O-atoms bridging uranyl polyhedra. The different average binding energies of the minerals of these groups indicate that the coordination environment of the equatorial O-atoms has a significant effect on the binding energy of the U 4f electrons. The O atoms in the first group occur as OH groups or O^{2-} in the second group as part of the (TO_n) groups, and in the third group either as part of the (TO_n) groups or as O^{2-} or OH^- (as in zippeite).

The $(OH)^-$, O^{2-} and (TO_n) groups can be distinguished by their Lewis basicity, which is a measure of their electrophilic strength; i.e. their ability to accept electrons. Brown (2002) lists the Lewis basicities of the complex oxyanions $(SiO_4)^{4-}$, $(PO_4)^{3-}$, $(CO_3)^{2-}$ and $(SO_4)^{2-}$ as 0.33, 0.25, 0.22 and 0.17 vu, respectively. These values were calculated using an average coordination number of [4] for the O-atoms of these anion groups in inorganic structures. Brown (2002) also showed that the coordination of an individual O-atom varies over a large range and that no characteristic Lewis basicity can be assigned to an individual O-atom. However, the coordination numbers of O in O^{2-} or (OH) groups in the equatorial plane of polymerized uranyl polyhedra vary only between [3] and [4]. Using the latter coordination number, the Lewis basicities of the O^{2-} and (OH) groups are 0.50 and 0.40 vu, respectively.

The XPS results given here show that the U^{6+} band of the U $4f_{7/2}$ peak shifts to higher-energy with a decrease in Lewis basicity of the anion group; i.e. from 381.3 eV for OH/O^{2-} groups to 381.6 eV for $O^{2-}/(TO_n)$ groups to 382.0 eV for (TO_n) groups. Fig. 7 shows that the binding

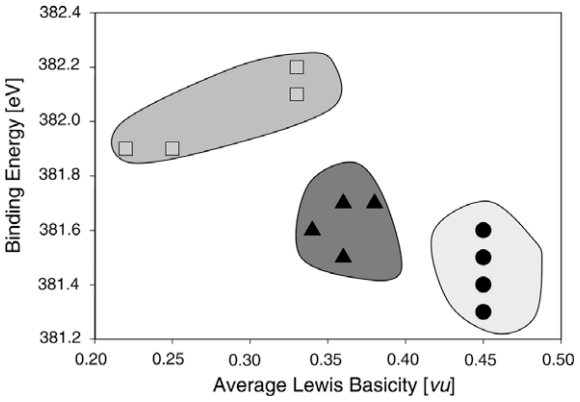

Fig. 7. The binding energy of the U^{6+} band in the U $4f_{7/2}$ peak versus the average Lewis basicity of the anion groups in the structural unit of uranyl minerals with divalent cations; data for uranyl oxysalts with (TO_n) groups are shown as squares, for oxysalts with (TO_n) groups and O^{2-} or (OH) groups as triangles, and for uranyl-hydroxy-hydrates as circles.

energies of the U^{6+} bands in U $4f_{7/2}$ peaks of minerals with divalent cations inversely correlate with the corresponding average Lewis basicities of the anion groups in the structural unit. This general trend results from the increase in covalency of the U—O bond with increasing Lewis basicity of the anion group. An increase in covalency of the equatorial bond results in a shift in electron density from O to U, which increases the electron density around U and thus decreases the binding energy of the photoelectrons.

5.2. Binding-energy shift in the U $4f_{7/2}$ spectra of uranyl-hydroxy-hydrate minerals

We described above the shift in binding-energy of the U^{6+} band from <382.1> eV for uranyl-hydroxy-hydrates with zero or small amounts of monovalent interstitial cations to <381.3> eV for the uranyl-hydroxy-hydrate minerals with divalent interstitial cations. Uranyl-hydroxy-hydrates with divalent cations have a higher number of stronger equatorial Lewis base O^{2-} than uranyl-hydroxy-hydrates with zero or small amounts of monovalent interstitial cations. Hence, there must be a shift to higher binding-energies with an increasing number of the weaker Lewis Base $(OH)^-$. However, this shift will be small in comparison to the shift of the U^{6+} band from uranyl-hydroxy-hydrates with divalent cations (<381.3>) to uranyl-oxy-salt minerals in which all equatorial O-atoms are shared with (TO_n) (<382.0>). Hence, the higher number of (OH) groups in the polymerized sheets of uranyl-polyhedra of the uranyl-hydroxy-hydrates with zero or small amounts of monovalent interstitial cations cannot solely explain the shift in binding energy from <381.3> to <382.1> eV.

In uranyl-hydroxy-hydrates with divalent interstitial cations, the latter cations bond either to O-atoms of the uranyl-groups or they bond to (H_2O) groups in the interlayer. These (H_2O) groups distribute the bond-valence from the interstitial cations and from (OH) groups of the structural unit throughout the interlayer to O-atoms of uranyl-groups. In uranyl-hydroxy-hydrate minerals without interstitial cations, the bond-valence emanated solely by the (OH) groups of the structural unit must be transferred to O-atoms of the uranyl-groups. Hence, the bond-valence sum accepted by the O-atoms of the uranyl-groups is smaller in uranyl-hydroxy-hydrate minerals without interstitial cations than in those with divalent cations.

Consider the uranyl-hydroxy-hydrate minerals metaschoepite, $[(UO_2)_4O(OH)_6](H_2O)_5$ and the endmember composition of fourmarierite, $Pb(H_2O)_4[(^{[7]}UO_2)_6O_3(OH)_4]$. Both minerals have sheets of polymerized uranyl-polyhedra with the same topology and they contain similar numbers of (H_2O) groups. However, fourmarierite has a higher number of the stronger Lewis Base O^{2-} and there is a greater transfer in bond-valence from the interstitial species Pb and H_2O to the O-atoms of the uranyl-groups. Closer examination of the structure of fourmarierite and metaschoepite shows that the greater transfer in bond-valence to O-atoms of the uranyl-groups results in an increase in the average bond-length of the uranyl-ion from <1.78 Å> in metaschoepite to <1.82 Å> in fourmarierite (with one Pb per formula unit, Li and Burns, 2000). These average bond-lengths correspond to bond-valences of 1.68 and 1.55 vu, respectively. This shows that an increase in the accepted bond-valence by the O-atoms of the uranyl-groups decreases the covalency of the uranyl-bond. One might expect a decrease in the electron density around U^{6+} with decreasing covalency of the uranyl-bond, similar to what we have concluded for the equatorial bonds (see above), however, this is not the case for the uranyl-bond.

There has been many reports and reviews on the electronic structure of the uranyl-bond (e.g. Denning 2007 and references therein). The following four molecular orbitals are involved in the bonding between U and O: $3\sigma_g$, $3\sigma_u$, $1\pi_g$ and $2\pi_u$, which suggests a notional U—O bond of the order of three (Denning, 2007). Experimental and theoretical studies show that an increase in bond-length of the U=O bond and thus a decrease in covalency are the result of the excitation of bonding electrons from $3\sigma_g$ or $2\pi_u$ to non-bonding U 5f orbitals (Denning 2007). Hence, an increase in the bond-length of U=O from metaschoepite to fourmarierite corresponds to an increase in the electron density around U^{6+}, explaining the lower binding energy of the U 4f electrons in fourmarierite than metaschoepite.

The following trends support the inverse correlation between the length of the uranyl-bond and the binding energy of the U 4f electrons for uranyl-hydroxy-hydrates:

(1) The length of the uranyl-bond increases from 1.65 to 1.78 Å for uranyl-hydroxy-hydrate minerals with no or monovalent interstitial cations (U^{6+} band at 382.0–382.3 eV) to 1.79–1.83 Å for uranyl-hydroxy-hydrate minerals with divalent interstitial cations (U^{6+} band at 381.0–381.6 eV).
(2) The lowest average U=O bond-length (1.65 Å) occurs in β-[$^{[6]}$UO2(OH)2] with a U^{6+} band at 382.3 eV and the highest average bond-length (1.83 Å) occurs in masuyite with a U^{6+} band at 381.1 eV.

The inverse correlation between the binding energy of the U^{6+} band and the length of the uranyl-bond does not necessarily apply, if one considers two uranyl-hydroxy-hydrate minerals with divalent cations and with polymerized sheets of different composition and topology. For example, the average bond-lengths of the uranyl-bond in becquerelite and fourmarierite are 1.79 and 1.82 Å, whereas the binding energies of the U^{6+} bands are <381.2> (synthetic and natural becquerelite) and 381.4 (fourmarierite), respectively. However, actual bond-lengths of the uranyl-bonds on surfaces may differ from those of bulk structures and therefore differences between average bond-lengths of uranyl-bonds may be larger or smaller on the surfaces of the corresponding minerals. This may be especially true for uranyl-hydroxy-hydrate minerals, which can loose significant amounts of (H_2O) groups in Ultra-High Vacuum (Schindler et al., 2009).

We can summarize that the Lewis basicity of the equatorial ligands O^{2-} and (OH) and the accepted bond-valence by the O-atoms of the uranyl bonds are two structural parameters that explain the differences in binding energies between uranyl-hydroxy-hydrates. Other potential factors could be structural factors such as the coordination number of U, the number of adjacent uranyl-polyhedra, surface features such as roughness (i.e. number of underbonded O-atoms) and hydrated or dehydrated surface layers.

5.3. U components in uranyl-hydroxy-hydrate minerals without divalent cations

As described above, the U 4f spectra of metaschoepite and Na-substituted metaschoepite contain a second U^{6+} band. This band occurs at a similar binding energy as the U^{6+} bands in the U 4f spectra of uranyl-hydroxy-hydrate minerals with divalent cations. To understand the occurrence of this band, we must consider the following facts:

(1) This band has not been reported for the U 4f spectrum of the metaschoepite powder-sample measured by Froideval et al. (2003).
(2) The corresponding crystals of metaschoepite and Na-substituted metaschoepite were too small for the preparation of a freshly cleaved surface and rather were washed with distilled water in order to remove any dust particles;
(3) Metaschoepite can either dehydrate to "dehydrated schoepite" or hydrate to schoepite (Finch et al., 1998). Note that dehydration or hydration processes of Na-substituted metaschoepite have not yet been explored.
(4) The U 4f spectra of α- and β-$UO_2(OH)_2$ do not contain this band;
(5) Both $UO_2(OH)_2$ phases can neither loose nor gain (H_2O) groups during heating or being exposed to water (Finch et al., 1998).

These facts suggest that the two U^{6+} bands in the U 4f spectra of metaschoepite and Na-substituted metaschoepite represent U species in structural environments of different hydration states. Different hydration states have not been observed for α- and β-$UO_2(OH)_2$, which would explain the absence of two U^{6+} bands in their U 4f spectra.

We conducted various experiments on the crystals of Na-substituted metaschoepite, because we initially assigned the band at 381.3–381.4 eV to U^{5+} and we wanted to test if this band was a result of the Ultra-High Vacuum or bombardment of X-rays. We are now in the position to evaluate the results of these experiments under the perspective that different hydration states on the surface of the mineral might be the reason for two U^{6+} bands in the U $4f_{7/2}$ spectrum. Furthermore, we can use the results of the experiments to gain some more information on the possible valence of the band at 380.5 eV.

In the first experiment, we tried to remove the upper surface layers of the Na-substituted metaschoepite through etching of the single crystal in a 5-ml HCl solution of pH 2 for 2 min. Subsequent XPS examination shows small increases in the U^{6+} band at 381.3 eV and the band at 380.3–380.5 eV (Fig. 8a and b and Table 1). Second, we kept the Na-substituted metaschoepite crystal for 6 months in air. The XPS spectrum taken their after shows the absence of the small U^{6+} band at 381.3 eV, the occurrence of two large U^{6+} bands at 381.9 and 382.2 eV (Table 1) and a small fraction of the band at 380.3-380.5 eV (Fig. 8c). Third, we stored the crystal in the XPS instrument at 10^{-10} torr for 1 week and subsequently exposed the sample to X-rays for 10 h. The U $4f_{7/2}$ spectra taken before and after the treatment show a shift of all bands to higher binding energies (Fig. 8d and Table 1).

There are several observations that indicate that the band at 380.3–380.5 eV corresponds to U^{4+}:

(a) The species is very stable during treatment with acidic solutions and 6-month exposure in air, which, from our experience, does not apply to U^{5+};
(b) The corresponding band is 1.6 eV apart from the strongest U^{6+} band in the untreated sample and it is 1.6 and 1.4 eV apart from any U^{6+} band in the spectra taken after 6 months exposure in air and after long exposures to UHV and X-rays, respectively.

Finch et al. (1996) studied the effect of X-rays on single crystals of schoepite. They showed that single crystal transform into a polycrystalline powder, involving a change in the appearance from translucent yellow to opaque yellow. Studies of the unit-cell parameters after exposure to X-rays showed a decrease in one of the unit-cell dimensions, which Finch et al. (1996) interpreted as transformation of schoepite into metaschoepite.

For Na-substituted metaschoepite, we also observed a change in the crystals appearance from translucent to opaque indicating that the UHV and bombardment by X-rays caused dehydration at the surface of the mineral. Simultaneous to the change in appearance occur a shift of all U-bands to higher binding energies and the disappearance of the small U^{6+} band at 381.3 eV (see above). These observations must be associated to the dehydration of the upper surface layers of Na-substituted metaschoepite, suggesting that the small

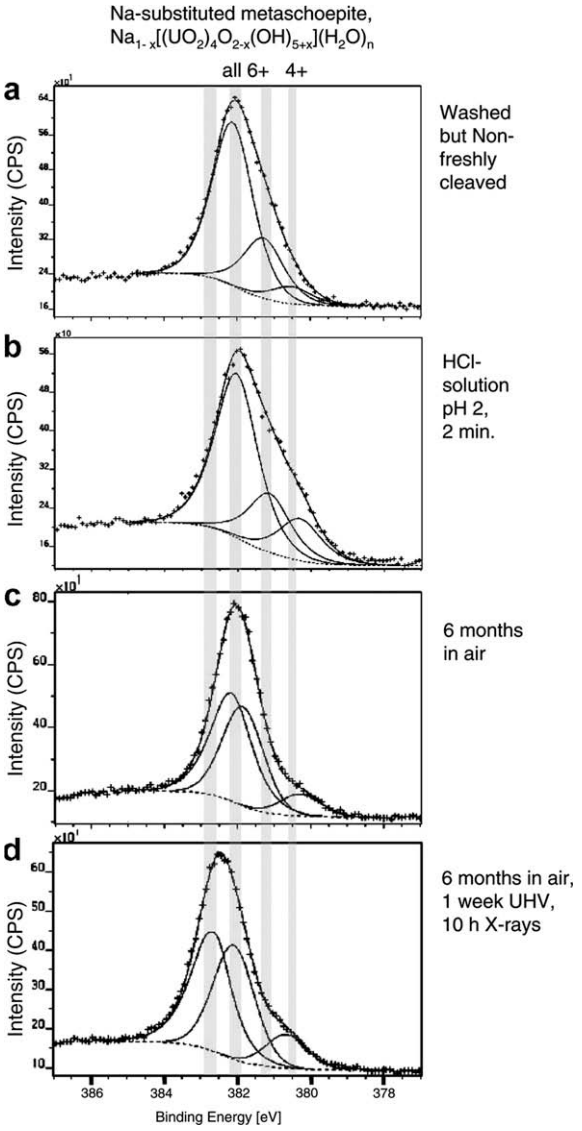

Fig. 8. The U $4f_{7/2}$ spectra for the same Na-substituted metaschoepite crystal after different types of treatment; the location of the U^{6+} and U^{4+} bands are indicated with vertical grey-shaded bars and the types of treatment are listed on the right-hand side. The thickness of the grey-shaded vertical bar indicates the variation in binding energy of the bands in the U $4f_{7/2}$ spectra.

U^{6+} band at 381.3 eV represents a higher hydrated U^{6+} species on the surface of the mineral (see also above). The reason for the shift in binding energies of the U-bands (i.e. a shift in electron density from U to O) must be related to structural changes inside the upper surface layers. These structural changes may be related again to a decrease in the U=O bond-length as a result of a decrease in the number of accepted bonds by the O-atoms of the uranyl-group.

5.4. Origin of U^{4+} and possible substitution mechanisms for U^{6+}

With the exception of ianthinite, $[U^{4+}{}_2(UO_2)_4O_6(OH)_4(H_2O)_4](H_2O)$ (Burns et al., 1997b) wyartite, $Ca(H_2O)_7[U^{5+}(UO_2)_2(CO_3)(O_4)(OH)]$ (Burns and Finch, 1999) and dehydrated wyartite, $Ca(CO_3)[U^{5+}(UO_2)_2O_4(OH)](H_2O)_3$ (Hawthorne et al., 2006), uranyl minerals contain U with a formal valence of 6+. The incorporation of lower-valent radionuclides such as Np^{5+} and Pu^{4+} into the structure of uranyl minerals is possible, but is presumably limited due by local charge-balance requirements (Burns et al., 1997a, 2004; Chen et al., 1999, 2000; Burns and Li 2002; Douglas et al., 2005; Burns and Klingensmith, 2006). The following question arises: how is it possible that the surfaces of some of the minerals examined contain small amounts of U^{4+} species? This could result from the conditions during formation of the uranyl minerals and compounds. For example, Finch and Ewing (1992) showed that uranyl minerals such as uranophane form as alteration products on the surface of uraninite, UO_2. At the mineral–water interface of such a U^{4+} mineral, the activity of U^{4+} is higher than in cases where uranyl minerals form at a larger distance from the primary U^{4+}-mineral. Hence, one might expect that uranyl minerals formed on the surface of U^{4+} minerals always incorporate a certain amount of U^{4+} into their structures. Another possibility is that crystals nucleate around uraninite precursors and therefore still contain small inclusions of uraninite crystals. The latter case might be especially true for minerals such as ianthinite, uranophane and schoepite, which are common oxidation products of uraninite (Finch and Ewing, 1992).

The incorporation of U^{4+} into the structural unit may be charge-balanced by (1) protonation of equatorial O-atoms of uranyl polyhedra, (2) protonation of two apical O-atoms bonding to U^{4+}, and (3) incorporation of interstitial cations (M) in the interlayer:

$$U^{6+}\text{—}O\text{—}2U^{6+} + 2e^- + 2H^+ \rightarrow 2U^{6+}\text{—}OH\text{—}U^{4+}\text{—}OH\text{—}2U^{6+} \quad (1)$$

$$O{=}U^{6+}{=}O + +2e^- + 2H^+ \rightarrow HO\text{—}U^{4+}\text{—}OH \quad (2)$$

$$M\text{—}O{=}U^{6+}{=}O + e^- + 2M^+ \rightarrow M^+\text{—}O\text{—}U^{4+}\text{—}O\text{—}2M^+ \quad (3)$$

where U^{6+}—O—$2U^{6+}$ is an equatorial O-atom bonding to three U^{6+}, O=U^{6+}=O is a uranyl-group, HO—U^{4+}—OH is a group of two apical OH groups bonding to U^{4+} and M—O—U^{4+}—O—$2M^+$ is a group of two apical O atoms bonding to U^{4+} and three M^+ cations.

There is also the possibility of the incorporation of U^{4+} into the interstitial complex, which would require deprotonation of the equatorial OH-groups. In the case of a uranyl mineral with a divalent interstitial cation, the incorporation could be charge-balanced in the following way:

$$M^{2+}\text{—}\left[U^{6+}\text{—}(OH)_2\text{—}U^{6+}\right] \rightarrow U^{4+}\text{—}\left[U^{6+}\text{—}O_2\text{—}U^{6+}\right] \quad (4)$$

where, $[U^{6+}\text{—}(OH)_2\text{—}U^{6+}]$ and $[U^{6+}\text{—}O_2\text{—}U^{6+}]$ represent the structural unit, and M^{2+} and U^{4+} represent the interstitial cations. Each of these charge-balancing mechanisms requires a modified structural environment around the incorporated lower-valent cation. The structural modifications may be limited, depending on the structure type of the corresponding mineral. However, there are fewer limitations of the incorporation of a lower-valent cation on a

surface, because in this environment charge balance can occur through protonation or deprotonation of underbonded O-atoms along terraces, steps and kinks.

6. CONCLUSIONS

XPS examination of the binding energies of the U $4f_{7/2}$ peak in uranyl minerals of different structures and chemical compositions showed that the presence of alkaline-earth cations in the interlayer and the coordination environment of equatorial O-atoms in the uranyl-polyhedra have a significant effect on the chemical shift of the U 4f peak. In the XPS spectra of uranyl minerals containing divalent cations, the U 4f peak shifts to higher binding energy with a decrease in the Lewis basicity of the equatorial oxy-groups; i.e. from O^{2-} and OH to oxy-anions such as $(SiO_4)^{4-}$, $(CO_3)^{2-}$, $(PO_4)^{3-}$ and $(SO_4)^{2-}$. In the spectra of uranyl-hydroxy-hydrate minerals with and without divalent interstitial cations, the bands shift to lower binding energies with lengthening of the uranyl bonds as result of an increase in bond-valence transfer from interstitial species to the O-atoms of the uranyl group.

The XPS spectra of uranyl minerals and synthetic compounds show the presence of U^{4+}, which may be the result of (1) a high activity of U^{4+} during the growth of the uranyl mineral and (2) the incorporation of uraninite crystals during growth. U 4f spectra of metaschoepite and Na-substituted metaschoepite contain two U^{6+} bands. The exposure of a Na-substituted metaschoepite crystal in air for 6 months and 1 week under UHV suggests that the smaller U^{6+} band at the lower binding energy side corresponds to a higher hydrated species on the surface of Na-substituted metaschoepite.

ACKNOWLEDGMENTS

This work was supported by a Canada Research Chair in Crystallography and Mineralogy and by a Discovery Grant to F.C.H. from the Natural Sciences and Engineering Research Council of Canada. M.S.F. were supported by a Canada Research Chair in conducting polymers. M.S.F. and F.C.H. are supported by a CFI Grant for surface science at the University of Manitoba. Furthermore, we thank Karrie-Ann Hughes, Amanda Klingensmith and Valery Gross for providing synthetic samples of becquerelite and Na-substituted metaschoepite. We are also thankful to Associate Editor David Vaughan, anonymous reviewers for their comments on earlier versions of the Manuscript and Jennifer Durocher for her help regarding final revisions.

REFERENCES

Allen G. C., Griffiths A. J. and Lee B. J. (1978) X-ray photoelectron spectroscopy of alkaline earth metal uranate. *Trans. Metal Chem.* **3**, 229–233.

Allen G. C. and Holmes N. R. (1987) Surface characterisation of α-, β-, γ-, and δ-UO_3 using X-ray photoelectron spectroscopy. *J. Chem. Soc. Dalton Trans.* 3009–3015.

Allen G. C. and Holmes N. R. (1993) Mixed valency behaviour in some uranium oxides studies by X-ray photoelectron spectroscopy. *Can. J. Appl. Spec.* **38**, 124–130.

Amayri S., Reich T., Arnold T., Geipel G. and Bernhard G. (2005a) Spectroscopic characterization of alkaline earth uranyl carbonates. *J. Solid State Chem.* **178**, 567–577.

Amayri S., Arnold T., Reich T., Foerstendorf H., Geipel G., Bernhard G. and Massanek A. (2005b) Spectroscopic characterization of the uranium carbonate Andersonite $Na_2Ca[(UO_2)(CO_3)_3]\cdot 6H_2O$. *Environ. Sci. Technol.* **38**, 6032–6036.

Bera S., Sali S. K., Sampath S., Narasimhan S. V. and Venugopal V. (1998) Oxidation state of uranium: an XPS study of alkali and alkaline earth uranates. *J. Nucl. Mater.* **255**, 26–33.

Brown I. D. (2002) The chemical bond in inorganic chemistry: the bond valence model. In *IUCr Monographs on Crystallography*. Oxford University Press.

Burns P. C. (1999) The crystal chemistry of uranium. *Rev. Mineral.* **38**, 23–90.

Burns P. C. (2005) U^{6+} Minerals and inorganic compounds: insights into an expanded structural hierarchy of crystal structures. *Can. Mineral.* **43**, 1839–1894.

Burns P. C., Miller M. L. and Ewing R. C. (1996) U^{6+} minerals and inorganic phases: a comparison and hierarchy of structures. *Can. Mineral.* **34**, 845–880.

Burns P. C., Ewing R. C. and Miller M. L. (1997a) Incorporation mechanisms of actinide elements into the structures of U^{6+} phases formed during the oxidation of spent nuclear fuel. *J. Nucl. Mater.* **45**, 1–9.

Burns P. C., Finch R. J., Hawthorne F. C., Miller M. L. and Ewing R. C. (1997b) The crystal structure of ianthinite, $[U^{4+}{}_2(UO_2)_4O_6(OH)_4(H_2O)_4](H_2O)_5$: a possible phase for Pu^{4+} incorporation during the oxidation of spent nuclear fuel. *J. Nucl. Mater.* **249**, 199–206.

Burns P. C. and Finch R. J. (1999) Wyartite: crystallographic evidence for the first pentavalent uranium mineral. *Am. Mineral.* **84**, 1456–1460.

Burns P. C. and Hanchar J. M. (1999) The structure of masuyite, $Pb[(UO_2)_3O_3(OH)_2]$ $(H_2O)_3$, and its relationship to protasite. *Can. Mineral.* **37**, 1483–1491.

Burns P. C. and Li Y. (2002) The structures of becquerelite and Sr-exchanged becquerelite. *Am. Mineral.* **87**, 550–557.

Burns P. C., Deely K. M. and Hayden L. A. (2003) The crystal chemistry of the zippeite group. *Can. Mineral.* **41**, 687–706.

Burns P. C., Deely K. M. and Skanthakumar S. (2004) Neptunium incorporation into uranyl compounds that form as alteration products of spent nuclear fuel: implications for geologic repository performance. *Radiochim. Acta* **92**, 151–159.

Burns P. C. and Klingensmith A. L. (2006) Uranium mineralogy and neptunium mobility. *Elements* **2**, 351–356.

Castle J. E. (2002) A wizard source of expertise in XPS. *Surf. Interf. Anal.* **33**, 196–202.

Castle J. E. and Salvi A. M. (2001) Interpretation of the Shirley background in X-ray photoelectron spectroscopy analysis. *J. Vacuum Sci. Technol.* **A19**, 1170–1175.

Chen F., Burns P. C. and Ewing R. C. (1999) ^{79}Se: geochemical and crystallo-chemical retardation mechanisms. *J. Nucl. Mater.* **275**, 81–94.

Chen F., Burns P. C. and Ewing R. C. (2000) Near-field behavior of ^{99}Tc during the oxidative alteration of spent nuclear fuel. *J. Nucl. Mater.* **278**, 225–232.

Clark J. R. (1960) X-ray study of alteration in the uranium mineral wyartite. *Am. Mineral.* **45**, 200–208.

Cooper M. A. and Hawthorne F. C. (2001) Structure, topology and hydrogen bonding in marthozite, $Cu^{2+}[(UO_2)_3(SeO_3)_2O_2](H_2O)_8$, a comparison with guilleminite, $Ba[(UO_2)_3(SeO_3)_2O_2](H_2O)$. *Can. Mineral.* **39**, 797–807.

Demartin F., Gramaccioli C. M. and Pilati T. (1992) The importance of accurate crystal structure determination of

uranium minerals. II. Soddyite $(UO_2)_2(SiO_4)\cdot 2H_2O$. *Acta Crystallogr.* **C48**, 1–4.

Denning R. G. (2007) Electronic structure and bonding in actinyl ions and their analogs. *J. Phys. Chem.* **111**, 4125–4143.

Doniach S. and Sunjic M. (1970) Many-electron singularity in X-ray photoemission and X-ray line spectra from metals. *J. Phys.* **C3**, 285–291.

Douglas M., Clark S. B., Friese J. I., Arey B. W., Buck E. C., Hanson B. D., Utsunomiya S. and Ewing R. C. (2005) Microscale characterization of uranium(VI) silicate solids and associated neptunium(V). *Radiochim. Acta* **93**, 265–272.

Drot R., Simoni E., Alnot M. and Ehrhardt J. J. (1998) Structural environment of uranium (VI) and europium (III) species sorbed onto phosphate surfaces: XPS and optical spectroscopy studies. *J. Colloid Interf. Sci.* **205**, 410–416.

Finch R. J. and Ewing R. C. (1992) The corrosion of uraninite under oxidizing conditions. *J. Nucl. Mater.* **190**, 133–156.

Finch R. J., Cooper M. A., Hawthorne F. C. and Ewing R. C. (1996) The crystal structure of schoepite $[(UO_2)_8O_2(OH)_{12}](H_2O)_{12}$. *Can. Mineral.* **34**, 1071–1088.

Finch R. J., Hawthorne F. C. and Ewing R. C. (1998) Structural relations among schoepite, metaschoepite and dehydrated schoepite. *Can. Mineral.* **36**, 831–845.

Finch R.J., Buck E.C., Finn P.A. and Bates J.K. (1999) Oxidative corrosion of spent UO_2 fuel in vapour and dripping groundwater at 90 °C. In: Scientific Basis for Nuclear Waste Management XXII (eds. D. J. Wronliewicz and J. H. Lee), *Mater. Res. Soc. Symp. Proc.*, vol. 556. Materials Research Society, Warrendale, PA, pp.431-439. .

Finch R. J. and Murakami T. (1999) Systematics and paragenesis of uranium minerals. *Rev. Mineral.* **38**, 91–180.

Finch R. J., Burns P. C., Hawthorne F. C. and Ewing R. C. (2006) Refinement of the crystal structure of billietite, $Ba[(UO_2)_6O_4(OH)_6](H_2O)_7$. *Can. Mineral.* **44**, 1197–1206.

Finn P. A., Hoh J. C., Wolf S. F., Slater S. A. and Bates J. K. (1996) The release of uranium, plutonium, cesium, strontium, technetium and iodine from spent fuel under unsaturated conditions. *Radiochim. Acta* **74**, 65–71.

Froideval A., Del Nero M., Barillon R., Hommet J. and Mignot G. (2003) PH dependence of uranyl retention in a quartz/solution system: an XPS study. *J. Colloid Interf. Sci.* **266**, 221–235.

Frondel C. (1958) Systematic mineralogy of uranium and thorium. *US Geol. Surv. Bull.* **1064**, 400 p.

Gauthier G., Francois A., Deliens M. and Piret P. (1989) Famous mineral localities: the uranium deposit of the Shaba region, Zaire. *Mineral. Rec.* **20**, 265–304.

Ginderow D. (1988) Structure de l'uranophane alpha, $Ca(UO_2)_2(SiO_3OH)_2\cdot 5H_2O$. *Acta Crystallogr.* **C44**, 421–424.

Goldschmidt V. M. and Thomassen L. (1923) Crystal structure of natural and synthetic oxides of U, Th and Ce. *Skrifter utgitt Norske Videnskaps-Akademi, Oslo. 1: Math. Nat. Klasse* **5**, 1–48.

Hawthorne F. C., Finch R. J. and Ewing R. C. (2006) The crystal structure of dehydrated wyartite, $Ca(CO_3)[U^{5+}(UO_2)_2O_4(OH)](H_2O)_3$. *Can. Mineral.* **44**, 1379–1385.

Ilton E. S., Haiduc A., Cahill C. L. and Felmy A. R. (2005) Mica surfaces stabilize pentavalent uranium. *Inorg. Chem.* **44**, 2986–2988.

Ilton E. S., Boily J. F. and Bagus P. S. (2007) Beam induced reduction of U(VI) during X-ray photoelectron spectroscopy: The utility of the U 4f satellite structure for identifying uranium oxidation states in mixed valence oxides. *Surf. Sci.* **601**, 908–916.

Keller C. and Jorgensen C. K. (1975) Photoelectron spectra of uranium (V) in mixed oxides showing characteristic satellite signals. *Chem. Phys. Lett.* **32**, 397–400.

Klingensmith A. L., Deely K. M., Kinman W. S., Kelly V. and Burns P. C. (2007) Neptunium incorporation in sodium-substituted metaschoepite. *Am. Mineral.* **92**, 662–669.

Li Y. and Burns P. C. (2000) Investigations of crystal chemical variability in lead uranyl oxide hydrates. I: Curite. *Can. Mineral.* **38**, 727–735.

Locock A. J. and Burns P. C. (2003) Crystal structures and synthesis of the copper-dominant members of the autunite and meta-autunite groups: tobernite, zeunerite, metatorbernite and metazeunerite. *Can. Mineral.* **41**, 489–502.

Loopstra B. O., Taylor J. C. and Waugh A. B. (1977) Neutron powder profile studies of the gamma uranium trioxide phases. *J. Solid State Chem.* **20**, 9–19.

Mereiter K. (1982) The crystal structure of liebigite, $Ca_2UO_2(CO_3)_3\cdot 11H_2O$. *Tschermaks Mineral. Petrogr. Mitteil.* **30**, 277–288.

Nefedov V. I., Teterin Y. A., Reich T. and Nitsche H. (1996) Determination of interatomic distances in uranyl compounds on the basis of U $6p_{3/2}$-level splitting. *Dokl. Akad. Nauk* **348**, 634–636.

Nesbitt H. W., Bancroft G. M., Davidson R., McIntyre N. S. and Pratt A. R. (2004) Minimum XPS core-level line widths of insulators, including silicate minerals. *Am. Mineral.* **89**, 878–882.

Piret P. (1985) Structure cristalline de la fourmariérite, $Pb(UO_2)_4O_3(OH)_4\cdot 4H_2O$. *Bull. Minéral.* **108**, 659–665.

Santos B. G., Nesbitt H. W., Noël J. J. and Shoesmith D. W. (2004) X-ray photoelectron spectroscopy study of anodically oxidized SIMFUEL surfaces. *Electrochim. Acta* **49**, 1863–1873.

Schindler M., Mandaliev P., Hawthorne F. C. and Putnis A. (2006a) Dissolution of uranyl-hydroxy-hydrate mineraIs. I: Curite. *Can. Mineral.* **44**, 415–431.

Schindler M., Hawthorne F. C., Burns P. C. and Maurice P. A. (2006b) Dissolution of uranyl-hydroxy-hydrate minerals. II: Becquerelite. *Can. Mineral.* **44**, 1207–1225.

Schindler M., Hawthorne F. C., Halden N. M., Burns P. C. and Maurice P. A. (2007a) Dissolution of uranyl-hydroxy-hydrate minerals. III: Billietite. *Can. Mineral.* **45**, 945–962.

Schindler M., Hawthorne F. C., Burns P. C. and Maurice P. A. (2007b) Dissolution of uranyl-oxide-hydroxy-hydrate minerals. IV: Fourmarierite and synthetic $Pb_2(H_2O)[(UO_2)_{10}UO_{12}(OH)_6(H_2O)_2]$. *Can. Mineral.* **45**, 963–981.

Schindler M., Hawthorne F. C., Freund M.S. and Burns P.C. (this issue) XPS spectra of uranyl-minerals and synthetic uranyl compounds. II: The O 1s spectrum. *Geochim. Cosmochim. Acta*.

Schueneman R. A., Khaskelis A. I., Eastwood D., van Ooij W. L. and Burggraf L. W. (2003) Uranium oxide weathering: spectroscopy and kinetics. *J. Nucl. Mater.* **323**, 8–17.

Scott T. B., Allen G. C., Heard P. J. and Randell M. G. (2005) Reduction of U(VI) to U(IV) on the surface of magnetite. *Geochim. Cosmochim. Acta* **69**, 5639–5646.

Sherwood P. M. A. (1990) Data analysis in XPS and AES. *Practical Surface Analysis* (eds. D. Briggs and M. P. Seah), vol. 1. John Wiley and Sons, 657 p.

Shirley D. A. (1972) High-resolution X-ray photoemission spectrum of the valence bands of gold. *Phys. Rev.* **B5**, 4709–4714.

Sunder S., Cramer J. J and Miller N. H. (1996) Geochemistry of the Cigar Lake Uranium Deposit: XPS Studies. *Radiochim. Acta*, **74**, 303–307.

Szymanski J. T. and Scott J. D. (1982) A crystal structure refinement of synthetic brannerite UTi_2O_6 and its bearing on rate of alkaline-carbonate leaching of brannerite in ore. *Can. Mineral.* **20**, 271–280.

Taylor J. C. (1971) The structure of the α-form of uranyl hydroxide. *Acta Crystallogr.* **B27**, 1088–1091.

Taylor J. C. and Bannister M. J. (1972) A neutron diffraction study of the anisotropic thermal expansion of β-uranyl dihydroxide. *Acta Crystallogr. B* **28**, 2995–2999.

Teterin Y. A., Kulakov V. M., Baev A. S., Nevzorov N. B., Melnikov I. V., Streltsov V. A., Mashirov L. G., Suglobov D. N. and Zelenkov A. G. (1981) A study of synthetic and natural uranium oxides by X-ray photoelectron spectroscopy. *Phys. Chem. Miner.* **7**, 151–158.

Teterin Y. A., Utkin I. O., Melnikov I. V., Lebedev A. M., Teterin A. Y., Ivanov K. E., Nikitin A. S. and Yukchevich L. (2000) X-ray photoelectron study of thorium silicate $ThSiO_4{\cdot}nH_2O$ and uranium silicate $USiO_4{\cdot}nH_2O$. *J. Struct. Chem.* **41**, 965–971.

Tougaard S. (1996) Quantitative XPS: non-destructive analysis of surface nano-structures. *Appl. Surface Sci.* **100**(101), 1–10.

Van den Berghe S., Laval J. P., Gaudreau B., Terryn H. and Verwerft M. (2000) XPS investigations on cesium uranates: mixed valency behaviour of uranium. *J. Nucl. Mater.* **277**, 28–36.

Veal B. W., Lam D. J., Carnall W. T. and Hoekstra H. R. (1975) X-ray photoemission spectroscopy study of hexavalent uranium compounds. *Phys. Rev.* **B12**, 5651–5663.

Vision 2.2.6 (2006) Kratos Analytical Ltd., Manchester, United Kingdom.

Viswanathan K. and Harneit O. (1986) Refined crystal structure of β-uranophane $Ca(UO_2)_2(SiO_3OH)_2{\cdot}5H_2O$. *Am. Mineral.* **71**, 1489–1493.

Wagner C. D, Riggs W. M., Davis L. E., Moulder J. F. and Mailenberg G. M (1979) *Handbook of X-ray Photoelectron Spectroscopy*. Perkin-Elmer.

Weller M. T., Light M. E. and Gelbrich T. (2000) Structure of uranium(VI) oxide dehydrate, $UO_3{\cdot}2H_2O$; synthetic metaschoepite, $(UO_2)_4O(OH)_6{\cdot}5H_2O$. *Acta Crystallogr.* **B56**, 577–583.

Wersin P., Hochella, Jr., M. F., Persson P., Redden G., Leckie J. O. and Harris D. (1994) Interaction between aqueous U(VI) and sulfide minerals: spectroscopic evidence of sorption and reduction. *Geochim. Cosmochim. Acta* **58**, 2829–2843.

Wronkiewicz D. J., Bates J. K., Gerding T. J., Veleckis E. and Tani B. S. (1992) Uranium release and secondary phase formation during unsaturated testing of UO_2 at 90 °C. *J. Nucl. Mater.* **190**, 107–127.

Wronkiewicz D. J., Bates J. K., Wolf S. F. and Buck E. C. (1996) Ten year results from unsaturated drip tests with UO_2 at 90 °C: implications for the corrosion of spent nuclear fuel. *J. Nucl. Mater.* **238**, 78–95.

Associate editor: David J. Vaughan